Epitaxial Graphene on SiC(0001): More than Just Honeycombs

Y. Qi, S. H. Rhim, G. F. Sun, M. Weinert, and L. Li*

Department of Physics and Laboratory for Surface Studies, University of Wisconsin, Milwaukee, Wisconsin 53211, USA

(Received 12 January 2010; revised manuscript received 19 May 2010; published 19 August 2010)

Using scanning tunneling microscopy with Fe-coated W tips and first-principles calculations, we show that the interface of epitaxial graphene/SiC(0001) is a warped graphene layer with hexagon-pentagon-heptagon ($H_{5,6,7}$) defects that break the honeycomb symmetry, thereby inducing a gap and states below E_F near the K point. Although the next graphene layer assumes the perfect honeycomb lattice, its interaction with the warped layer modifies the dispersion about the Dirac point. These results explain recent angle-resolved photoemission and carbon core-level shift data and solve the long-standing problem of the interfacial structure of epitaxial graphene on SiC(0001).

DOI: 10.1103/PhysRevLett.105.085502 PACS numbers: 61.48.Gh, 68.37.Ef, 71.20.−b, 73.22.Pr

Graphene, a one-atom-thick planar sheet of sp^2-bonded carbon atoms in a honeycomb lattice, is the building block of many carbon allotropes. The strong in-plane σ bonds form the backbone of the honeycomb, while the half-filled π bonds exhibit linear band dispersion near the K points [1]. This unique construct leads to graphene's novel physical and electronic properties such as room temperature (RT) quantum Hall effects, Klein tunneling, and high carrier mobility [2–4]. Recently, uniform wafer-sized graphene has been grown epitaxially on hexagonal SiC [5] and transition metal substrates [6,7], a critical step towards the development of graphene electronics [8,9].

Nevertheless, the mismatch with the SiC substrate can have profound effects on the physical and electronic properties of epitaxial graphene. On the $(000\bar{1})$ C face, the formation of a ''twisted'' interface leads to the decoupling between different layers of multilayer graphene, each behaving as a single layer with a carrier mobility of 250 000 $\mathrm{cm}^2/\mathrm{V\,s}$ [10,11], comparable to that of exfoliated graphene [4]. On the (0001) Si face, however, the picture remains controversial [12]. Structurally, graphitization has been known since 1975 to start with a $(6\sqrt{3} \times 6\sqrt{3})$ structure [13], which remains at the interface during subsequent layer growth. While earlier studies suggested that it consisted of graphene layers weakly bonded to either the (1×1) SiC(0001) surface [13,14] or Si-rich interface layers [15–17], recent work indicates a carbon layer covalently bonded to the SiC [18–23]. Another hotly debated issue is the origin of the gap near the K points observed by angle-resolved photoemission spectroscopy (ARPES)—a property crucial for its use in electronic devices [24–26]—but found only for the Si face, and absent for the C face and exfoliated graphene.

In this Letter, we show that these unique properties of epitaxial graphene on the Si face arise from a warped interfacial graphene layer, resulting from the periodic inclusion of hexagon-pentagon-heptagon ($H_{5,6,7}$) defects in the honeycomb to relieve the mismatch with the SiC substrate. The $H_{5,6,7}$ defects break the symmetry of the honeycomb, thereby inducing a gap: the calculated band structure of the proposed model along Γ-K is semiconducting with two localized states near K points below E_F, correctly reproducing the published photoemission and C $1s$ core-level spectra [22,23]. Furthermore, the next graphene layer assumes the defect-free honeycomb lattice, though its interaction with the warped layer leads to deviations from the linear dispersion at the Dirac point, shedding light on the origin of the observed anomalies in ARPES [25,26].

Experiments were carried out on epitaxial graphene grown on N-doped 6H-SiC(0001), which was first etched in a H_2/Ar atmosphere at 1500 °C. After annealing at ~950 °C for 15 min in a Si flux to produce a (3×3) reconstructed surface, the SiC substrate was heated to ~1300 °C to grow graphene in ultrahigh vacuum [27]. Scanning tunneling microscopy (STM) images were taken using W and functionalized W tips, where the latter are made by coating W tips with Fe at RT and followed by annealing at 500–700 °C in ultrahigh vacuum.

First-principles calculations, using the full-potential linearized augmented plane wave method as implemented in *flair* [28], model the substrate using a 3×3 6H-SiC(0001) 6-bilayer supercell, with a vacuum region of ~20–25 Å and a basis cutoff of ~195 eV. Because of the usual density functional theory underestimation of the gap (1.6 vs 3.0 eV for 6H-SiC), comparisons of calculated density of states (DOS) and STM images are limited to biases within $E_F \pm 0.5$ eV.

Figure 1 presents an STM image of the $(6\sqrt{3} \times 6\sqrt{3})$ graphene/SiC(0001) interface, and closeups of the two main features observed: an up-pointing trimer marked by a triangle of sides ~3.5 ± 0.2 Å, and a rosette marked by a hexagon of sides ~3.2 ± 0.2 Å. While the appearance of the trimer is bias independent, the contrast of the rosette is slightly less in empty-state images. The ratio of trimer to rosette depends on growth conditions, but the former is always more populated. The image shown in Fig. 1(a), taken at an early stage of growth (the Si-rich $\sqrt{3}$ reconstruction still can be seen on part of the surface), shows a trimer-to-rosette ratio of ~2:1. Higher ratios (e.g., 4:1) are

 © 2010 The American Physical Society

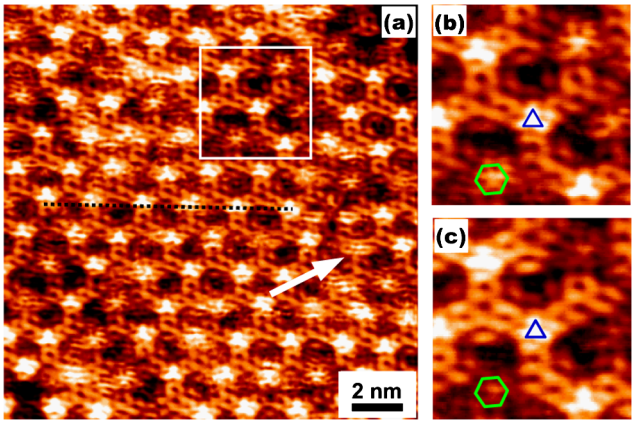

FIG. 1 (color online). (a) STM image of epitaxial graphene on 6H-SiC(0001) taken with an Fe-coated W tip at sample bias $V_s = -0.1$ V, tunneling current $I_t = 0.3$ nA. Expanded views of marked features taken at (b) -0.1 V and (c) $+0.1$ V. Image size: 4.5×4.5 nm^2. The arrow marks a common defect likely associated with Si vacancies in the substrate.

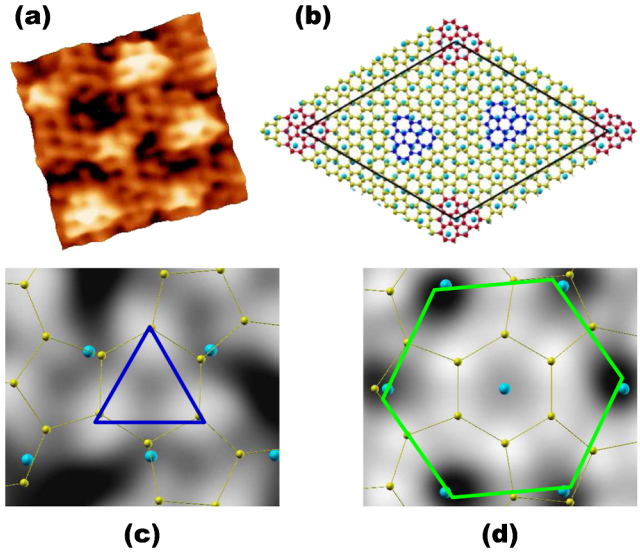

FIG. 2 (color online). (a) An STM image taken with an Fe/W tip at sample bias -0.5 V and $I_t = 0.4$ nA, size $= 4 \times 4$ nm^2. (b) Proposed model for the $(6\sqrt{3} \times 6\sqrt{3})$ structure with top and hollow variants. The $H_{5,6,7}$ defects can be placed into the graphene lattice without causing dislocations, thus naturally allowing for disordered arrangements, consistent with STM observations. Calculated DOS isosurfaces (10^{-6} a.u.$^{-3}$) for occupied states between -0.1 eV and the Fermi level for the (c) top and (d) hollow variants. Carbon atoms are represented by small balls; Si, by larger balls.

observed at later stages of growth, accompanied also by a greater number of defects. Close examination of images and line profiles (e.g., dashed line in Fig. 1) indicates: (1) neighboring features typically do not fall on the same line; (2) the spacing is nonuniform, averaging $\sim$19 Å, i.e., about $6\times$ the (1×1) lattice spacing of SiC(0001); and (3) the center of the rosettes consists of a downward pointing trimer, which can be better seen in 3D in Fig. 2(a).

STM images (not shown) of the $(6\sqrt{3} \times 6\sqrt{3})$ taken using W tips at larger bias (e.g., $E_F \pm 1.5$ eV) are similar to earlier studies [12,29–31]. Imaging at energies closer to E_F (within ± 0.1 eV) is challenging [29–31], but can be routinely achieved with Fe-coated W tips. Our modeling of the Fe/W tip indicates that the Fe minority spin channel has an especially sharp peak 0.5 eV below E_F, facilitating tunneling between the tip and graphene-specific states not accessible with conventional W tips. These images clearly reveal new details of the $(6\sqrt{3} \times 6\sqrt{3})$ structure that cannot be explained by existing models. For example, simulated STM images based on defect-free graphene covalently bonded to SiC(0001) (1×1) show features of only threefold or twofold symmetry [20,21]. In addition, most of these calculations indicate that $(6\sqrt{3} \times 6\sqrt{3})$ is metallic [18–20], rather than semiconducting around K as evident in ARPES [22,23]. A highly interacting graphene layer can yield a semiconducting gap [17], but requires complexes of Si tetramers and adatoms bonding to the SiC at the interface not seen in ARPES data at this stage of graphene growth [22].

Here, we propose a new interface model that accounts for STM, ARPES, and C core-level observations [22–25]. A (13×13) graphene lattice is nearly commensurate to $(6\sqrt{3} \times 6\sqrt{3})$ SiC(0001) [12], which results in two high symmetry positions: a C atom or a graphene hexagon centered above a Si. Our calculations indicate that C atoms located directly above Si are pulled towards the SiC surface such that the Si-C bond is shortened to 2.0 Å from a nominal interplanar separation of 2.3 Å, consistent with other calculations [21].

To better accommodate this bond distortion and retain the threefold coordination for each C atom, pentagons and heptagons—which cause positive and negative curvatures [32–34], respectively—can be inserted into the honeycomb lattice. Inclusion of three pairs of alternating pentagons and heptagons around a rotated hexagon ($H_{5,6,7}$) [Fig. 2(b)] significantly reduces the distortions of the C-C bonds, and preserves the long-range translational and rotational integrity of the graphene honeycomb. Placement of the $H_{5,6,7}$ defects at the two high symmetry positions leads to two variants. At the "top" site [Fig. 2(c)], three Si atoms sit directly below the corners of the central hexagon of the $H_{5,6,7}$, with this hexagon centered above a C of the SiC substrate. At the "hollow" sites [Fig. 2(d)], the central hexagon is centered over a Si, and three Si atoms are now bonded to C atoms at the edge of the $H_{5,6,7}$ defect. Overall, this transformation decreases interfacial Si-C bonds from 4 (6) to 3 at the hollow (top) sites, further reducing the mismatch with the SiC substrate. The result is a warped graphene layer covalently bonded to SiC(0001) (1×1), whose formation is favored by ~ 0.1 eV/C compared to a (relaxed) honeycomb structure, with the top site more stable than the hollow by 0.03 eV/C. (The calculated adhesion energy of the honeycomb layer, relative to isolated graphene, is slightly nonbinding by

~0.02 eV/atom.) These results are in contrast to unsupported graphene where the $H_{5,6,7}$ defect formation energy is ~5.1 eV; the stability of the warped layer on SiC(0001) is due to its ability to accommodate the strain induced by the Si-C interactions.

Calculated local DOS isosurfaces (corresponding to the STM constant current mode) for the two $H_{5,6,7}$ variants on SiC are shown in Figs. 2(c) and 2(d). For the top site [Fig. 2(c)], the sixfold symmetry of the center hexagon is broken by the formation of three Si-C bonds, leading to maxima at three adjacent alternating C atoms, appearing as a trimer of ~3 Å. For the hollow variant, depressions are seen within the three heptagons as well as at the three C atoms at the tips of the three pentagons, resembling the sixfold depressions [marked by the hexagons in Figs. 1(b) and 1(c)] seen by STM. Because the six depression sites are inequivalent, they do not coincide perfectly with the hexagon of ~3 Å, consistent with STM observations. The central three C atoms above the T_4 sites are slightly brighter, appearing as a downward trimer. Overall, the main features seen in the STM images are well reproduced in the calculations. (That the slight center depressions seen in the calculated images are not observed in the STM images may be attributed to (i) the calculations not explicitly including the structure of the tip, and (ii) the images are taken at RT.)

In our proposed model, the electronic structure is significantly altered. Thus, experimental ARPES results provide a stringent test of our and other models [18–21]. Although the system does not have the (1×1) graphene periodicity, the bands can still be "unfolded" into the (larger) graphene Brillouin zone by projecting the (supercell) wave functions onto the corresponding k of the (1×1) graphene cell. The calculated k-projected surface bands for the two $H_{5,6,7}$ variants are given in Figs. 3(a)–3(c). Both variants show definite gaps, i.e., are semiconducting along Γ-K. Compared to defect-free graphene, our model shows well-developed graphene-like σ bands shifted to greater binding energy and significant changes in the π-band region: (1) increased (diffuse) weight around Γ and (2) upward dispersing bands ending ~3 eV below E_F at K. Both variants have defect-induced states (marked by arrows in Fig. 3) with energies at K, ε(K), of about −0.9 and −1.8 eV for the hollow and top configurations, respectively. The dispersions of these states (whose intensities decrease significantly away from K) have a tight-binding behavior appropriate for a single-band of localized orbitals, $\varepsilon(\mathrm{K}) = \varepsilon_H$-$A$: the period of the oscillations seen in Figs. 3(b) and 3(c) reflect the 3×3 cell used in the calculations, while the amplitude $A \sim 0.3$ eV about the "on-site" energies ε_H (indicated by the horizontal lines) are a measure of the interactions among the $H_{5,6,7}$ defects. From tight-binding scaling arguments, the use of larger $6\sqrt{3} \times 6\sqrt{3}$ (or 6×6) cells would result in a decrease in A (and interactions) by at least an order of magnitude; i.e., our model predicts (almost dispersionless) states around K

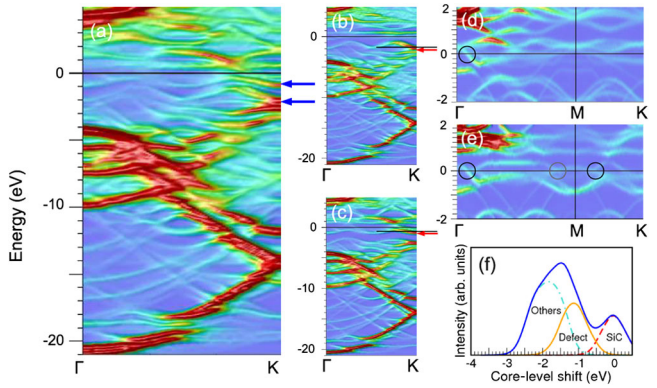

FIG. 3 (color online). Calculated k-projected surface bands (convoluted with a decaying exponential to account for the photoelectron escape depth) for the $H_{5,6,7}$ structure along Γ-K for (a) equal contributions of both variants, and (b) top and (c) hollow variants separately. Arrows mark the localized states at K and the lines in (b) and (c) indicate ε_H. Vacuum-weighted bands along Γ-M-K for (d) top and (e) hollow variants. (f) Calculated initial state 1s core-level shifts for different carbon atoms.

with energies $\varepsilon_H \approx -0.6$ and -1.5 eV, in excellent agreement with the experimental values of -0.5 and -1.6 eV [22,23]. The calculated bands along Γ-M similarly are in good agreement with the experimental ARPES spectra.

The apparent inconsistency, both experimentally and theoretically, between a gap along Γ-M and STM imaging at low bias can be understood by noting that STM probes the electronic states in the outer tails of the electronic distribution, whereas ARPES is sensitive to the overall wave function. In Figs. 3(d) and 3(e), the k-projected bands along Γ-M-K are shown for the two variants, but now weighted by the contributions in the vacuum region probed by STM. In both cases, the gap at K is still seen, but states elsewhere in the (1×1) zone cross E_F [such as those circled in Figs. 3(d) and 3(e)] are responsible for the contrast seen in STM images at low biases.

Calculated initial state C 1s core-level shifts [Fig. 3(f)], separated into contributions from the SiC substrate, the C atoms of the $H_{5,6,7}$ defect (-1.1 eV), and the rest of the C atoms (-1.8 eV), are consistent with experimental results [22,23]. Overall, the qualitative and quantitative agreement with the available experimental data for these defining properties of the $(6\sqrt{3} \times 6\sqrt{3})$ layer—the gap at K, the overall dispersion, the presence of the two localized states near K, and the C core-level shifts—provides significant support for our model of the graphene/SiC(0001) interface layer.

During the subsequent growth of graphene multilayers, as shown in Fig. 4(a), both the honeycomb and the interfacial structures (e.g., the trimers) can be clearly seen on the large terrace, while only a triangular lattice with a 2.5 Å spacing is observed on the smaller terrace in the lower right hand corner. This confirms that the warped graphene layer remains at the interface, and is still accessible by electron

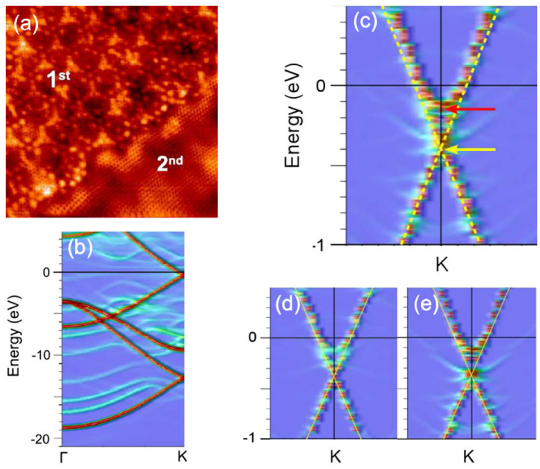

FIG. 4 (color online). (a) STM image taken with a W tip at sample bias $V_s = -0.9$ V, tunneling current $I_t = 1.2$ nA, image size $= 15 \times 15$ nm^2. (b) k-projected surface bands for the warped interface + first layer graphene on SiC(0001). (c) Bands around the Dirac point; (d) top and (e) hollow variants. The arrow at ~ -0.4 eV marks the (split) Dirac point and dotted lines are guides for the linear dispersion.

tunneling up to the first layer [12,17]. Calculations indicate that the first layer graphene is quite flat, and resumes the perfect honeycomb lattice spacing of 2.5 Å with an interlayer spacing of 3.2 Å relative to the warped interface layer. The k-projected band structure for the interface + first layer graphene [Fig. 4(b)] shows almost perfect graphene bands, with the Dirac point below E_F. The bottom of the $\sigma(\pi)$ band at Γ is shifted upwards by about 1.3 (3.5) eV compared to the interface (Fig. 3), qualitatively consistent with the ARPES data [22,23].

The bands near the Dirac point are shown in more detail in Figs. 4(c)–4(e). The downward shift of $E_D = -0.4$ eV indicates that the layer is n-doped, consistent with experiment [25,26]. The calculated splitting of the Dirac states is only 33 meV. However, because of the interactions with the warped interface graphene layer, there are deviations from the linear dispersion of defect-free graphene, leading to parabolic dispersion above the gap, and an apparent gap of $\sim$0.25 eV [marked by the arrows in Fig. 4(c)], closely matching the 0.26 eV gap reported in ARPES studies [25]. Comparison of Figs. 4(d) and 4(e) reveals subtle, but distinct differences in the dispersions, especially above the Dirac point, as a direct consequence of the different interactions between the first graphene layer and the two $H_{5,6,7}$ variants.

Closely related is the misalignment of the bands above and below E_D, illustrated by the dotted lines in Figs. 4(c)–4(e). The projections of the π states below E_D do not pass through the π^* states above E_D, an observation previously attributed to electron-phonon or electron-plasmon interactions [26]. (Shifting the lines upward, the dispersion of the π^* bands above E_D can be fit, but then misaligns the π states below E_D.)

In summary, the atomic structure of the graphene/SiC(0001) interface is found to be a warped graphene layer with the inclusion of $H_{5,6,7}$ defects in the honeycomb lattice, with the subsequent layer assuming the perfect honeycomb structure. Our results provide a consistent explanation of the available experimental data, and resolve a long-standing controversy regarding the interfacial structure of epitaxial graphene on SiC(0001), a material that may significantly impact the development of graphene electronics.

This work was supported by the U.S. DOE, Office of Basic Energy Sciences (DE-FG02-07ER46228).

*lianli@uwm.edu

[1] A. H. Castro Neto *et al.*, Rev. Mod. Phys. **81**, 109 (2009).
[2] D. L. Miller *et al.*, Science **324**, 924 (2009).
[3] N. Stander, B. Huard, and D. Goldhaber-Gordon, Phys. Rev. Lett. **102**, 026807 (2009).
[4] K. I. Bolotin *et al.*, Phys. Rev. Lett. **101**, 096802 (2008).
[5] K. V. Emtsev *et al.*, Nature Mater. **8**, 203 (2009).
[6] K. S. Kim *et al.*, Nature (London) **457**, 706 (2009).
[7] X. Li *et al.*, Science **324**, 1312 (2009).
[8] J. Kedzierski *et al.*, IEEE Trans. Electron Devices **55**, 2078 (2008).
[9] Y. M. Lin *et al.*, Nano Lett. **9**, 422 (2009).
[10] M. Sprinkle *et al.*, Phys. Rev. Lett. **103**, 226803 (2009).
[11] M. Orlita *et al.*, Phys. Rev. Lett. **101**, 267601 (2008).
[12] J. Hass, W. A. de Heer, and E. H. Conrad, J. Phys. Condens. Matter **20**, 323202 (2008).
[13] A. J. van Bommel, J. E. Crombeen, and A. van Tooren, Surf. Sci. **48**, 463 (1975).
[14] M.-H. Tsai *et al.*, Phys. Rev. B **45**, 1327 (1992).
[15] J. E. Northrup and J. Neugebauer, Phys. Rev. B **52**, R17001 (1995).
[16] I. Forbeaux, J.-M. Themlin, and J.-M. Debever, Phys. Rev. B **58**, 16396 (1998).
[17] G. M. Rutter *et al.*, Phys. Rev. B **76**, 235416 (2007).
[18] A. Mattausch and O. Pankratov, Phys. Rev. Lett. **99**, 076802 (2007).
[19] F. Varchon *et al.*, Phys. Rev. Lett. **99**, 126805 (2007).
[20] S. Kim *et al.*, Phys. Rev. Lett. **100**, 176802 (2008).
[21] F. Varchon *et al.*, Phys. Rev. B **77**, 235412 (2008).
[22] K. V. Emtsev *et al.*, Mater. Sci. Forum **556–557**, 525 (2007).
[23] K. V. Emtsev *et al.*, Phys. Rev. B **77**, 155303 (2008).
[24] K. S. Novoselov, Nature Mater. **6**, 720 (2007).
[25] S. Y. Zhou *et al.*, Nature Mater. **6**, 770 (2007).
[26] A. Bostwick *et al.*, Nature Phys. **3**, 36 (2007).
[27] L. Li and I. S. T. Tsong, Surf. Sci. **351**, 141 (1996).
[28] M. Weinert *et al.*, J. Phys. Condens. Matter **21**, 084201 (2009).
[29] P. Mallet *et al.*, Phys. Rev. B **76**, 041403(R) (2007).
[30] C. Riedl *et al.*, Phys. Rev. B **76**, 245406 (2007).
[31] P. Lauffer *et al.*, Phys. Rev. B **77**, 155426 (2008).
[32] D. Orlikowski *et al.*, Phys. Rev. Lett. **83**, 4132 (1999).
[33] J.-C. Charlier and G.-M. Rignanese, Phys. Rev. Lett. **86**, 5970 (2001).
[34] S. Ihara *et al.*, Phys. Rev. B **54**, 14713 (1996).